Zhang, Xiaochen and Li, Weili and Baoquan, Kou and Cao, Junci and Cao, Haichuan and Gerada, C. and Zhang, He (2014) Electrothermal combined optimization on notch in air-cooled high-speed permanent-magnet generator. IEEE Transactions on Magnetics, 51 (1). p. 8200210. ISSN 0018-9464

Electro-thermal combined optimization on notch in air cooled High Speed Permanent Magnetic Generator

Xiaochen Zhang[1], Weili Li[1], Baoquan Kou[2], Junci Cao[1], Haichuan Cao[2], Chris Gerada[3], He Zhang[3]

[1]School of Electrical Engineering, Beijing Jiaotong University, Beijing, 100044, China
[2] School of Electrical and Automation, Harbin Institute of Technology, Harbin, 150001 China
[3]School of Electrical Engineering, The University of Nottingham, Nottingham, NG7 2RD, UK

A 30kVA, 96000rpm, air cooled high-speed permanent magnetic generator (HSPMG) is investigated in this paper. Considering effects on both the magnetic circuit and heat transfer paths comprehensively, the stator slot notch in this HSPMG is optimized. First, by using the time-stepping finite element method, the transient electromagnetic fields of HSPMG is numerically calculated, and the electromagnetic losses in different components are obtained. Then, after the determination of other mechanical losses in such a machine, a three-dimensional fluid-thermal coupling calculation model is established, and the working temperature distribution in the HSPMG is studied. Thus, the electromagnetic-fluid-thermal coupling analysis method on the HSPMG is proposed, by using which the influences of machine notch height on machine magnetic circuit and cooling air flowing path are investigated. Meanwhile, both the electromagnetic performance and the temperature distribution in HSPMG with different stator notch height are studied, and a series of analytical equations are deduced to describe the variations of machine performances with stator notch. By using the proposed unbalance relative weighting method, the notch height is optimized to enhance the performance of HSPMG. The obtained conclusions could provide reference for HSPMG electromagnetic calculation, cooling system design, and optimization design.

***Index Terms*—High speed permanent magnetic generator, electromagnetic, thermal, fluid, optimization.**

I. INTRODUCTION

THE high-speed permanent magnet generator (HSPMG) is commonly used as the power generation equipment of Micro Turbine Power Generation System(MTPGS) [1-2]. HSPMG has many advantages, such as simple structure, high power density, no excitation loss, and high efficiency [3-4]. In addition, the HSPMG also has good application prospects in household appliances, aerospace, marine applications, and the flywheel energy storage systems, etc[5]. Thus, it has become the research focus of international electrical machines scholars.

The design of high-speed electrical machine is always a challenging task because of close interaction between the electromagnetic, mechanical and thermal issues. The high power density would cause higher losses and results in higher thermal load. The operating frequency of the HSPMG studied in this paper is 1600 Hz, and the induced eddy current in rotor metal sleeve is much higher than that of normal machines, which would affect the output performance and working temperature [6][7]. On the other hand, the high working temperatures of the machine will cause thermal demagnetization, and reduce the lifetime of rotor magnets [8].

The HSPMG adopt an open-type forced air cooling system, and the machine is fixed by the supporting ribs and is placed within the inlet channel of micro-turbine. The forced inlet air is flowing on the out surfaces of HSPMG shell and cooling the frame. Meanwhile, it also enters into the generator and cools the stator end windings, stator core, and rotor directly. Therefore, the topology structure, especially the air-gap and tooth slot shape, would not only have impacts on the magnetic circuit and machine output electromagnetic performance, but also affect the cooling path inside HSPM which influences the working temperature distribution directly .

Nowadays, many researchers devote to the performance improvement of HSPMG. Some scholars focus on the electromagnetic field calculation and losses analyses, and some important research results have been achieved [6-11]. Some scholars have analyzed the temperature distribution and thermal performance in HSPMG [12][13]. Some researchers have studied the methods for machines thermal analyses [14-16]. Some scholars make efforts on the optimization design of high-speed electric machines [17-19].

In this paper, a 30kVA air-cooling HSPMG is investigated. Considering the variations in both magnetic circuit and ventilation path of HSPMG caused by height of stator slot notch, a series of analytical equations to describe the variations of electromagnetic and the thermal performance are deduced from the electromagnetic-fluid-thermal coupling numerical analyses. After being reformed by using the non-equilibrium relative weighting method, the proposed electro-thermal objective function is combined optimized by the GA algorithm, and a best stator slot notch height is determined.

II. ELECTRICAL ANALYSIS AND LOSS DETERMINATION

The machine studied in this paper is a 30kVA air cooled HSPMG with a slender structure. Its rated operating speed is 96000 rpm, and the rated output voltage is 480 V, the core length is 120 mm, the outer diameter of the stator is 85 mm, and the rotor outer diameter is 32 mm.

The rotor is excited by the Permanent Magnets (PM) which are protected by a metal sleeve (50Mn18Cr5 [20]). The magnets are made of SM-26U [21], with magnetic retentively of 1.05 T and remanent flux density of 750 kA/m.

For the slender structure, the flux distribution variation along the axial is so small in HSPMG, that the magnetic field

Manuscript received January 1, 2014 Corresponding author: Weili Li (e-mail: wlli@bjtu.edu.cn).
Digital Object Identifier inserted by IEEE

in machines could be considered as a series of parallel plane field perpendicular to the axial direction. Thus, in this paper, only the two-dimensional (2-D) flux distribution in the cross section perpendicular to the axial direction is analyzed [19]. Considering the motor characteristics, and to reduce the error occurred during the two-dimensional electromagnetic analysis, the field-circuit coupling calculation method is adopted in this research. The stator end windings resistance and end windings leakage reactance are considered by adding a resistance and an inductance in the power circuit. However, the three-dimensional eddy current distribution is not considered, and eddy current loss in sleeve outside the core length region is neglected. Following assumptions are made.

i) The effects of displacement current is ignored.

ii) Hysteresis effect in permanent magnets is ignored.

iii) The leakage fluxes outside machine core are ignored.

To investigate the eddy current and eddy loss in rotor sleeve caused by high order harmonic components of armature magnetic field, the transient electromagnetic field of the HSPMG is analyzed by using the time stepping Finite Element Method. The determined mathematical model is described as (1), and the calculation region is shown in Fig.1.

$$\begin{cases} \Omega : \dfrac{\partial}{\partial x}\left(\dfrac{1}{\mu}\dfrac{\partial A_z}{\partial x}\right)+\dfrac{\partial}{\partial y}\left(\dfrac{1}{\mu}\dfrac{\partial A_z}{\partial y}\right)=-\left(J_z-\sigma\dfrac{\mathrm{d}A_z}{\mathrm{d}t}\right) \\ \Gamma_1 : A_z = 0 \\ \Gamma_2 : \dfrac{1}{\mu_1}\dfrac{\partial A_z}{\partial n}-\dfrac{1}{\mu_2}\dfrac{\partial A_z}{\partial n}=J_s \end{cases} \tag{1}$$

where Ω is the calculation region, A_z and J_z are magnetic vector potential and the source current density in the z-axial component, J_s is the equivalent surface current density of PM, σ is conductivity. Γ_1 is the parallel boundary condition, Γ_2 is the permanent magnet boundary condition, μ_1 and μ_2 are relative permeability.

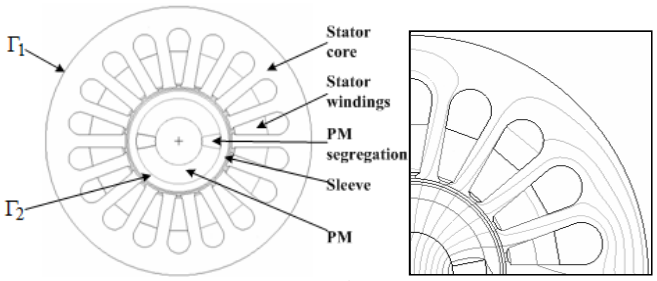

Fig. 1 Calculation region and the partial flux distribution in HSPMG.

Considering that the stator armature windings is composed of mush-wound coils and the diameter of the wire is 0.23 mm, the eddy loss and high frequency additional loss of stator windings are ignored in the analysis.

From the transient electromagnetic analyses, the flux and the vector magnetic potential distributions of the machine are obtained, as shown in Fig. 1. Then, the induced phase electromotive force could be calculated, which is taken into the equivalent circuit equations of synchronous machines, and the terminal voltage and armature current are determined.

Fig.2 shows the variations of machine voltage and armature current with time. Without the influences from outer connected current transformer, the output voltage and current are sinusoidal, and this can reduce the induced eddy loss in rotor sleeve effectively. The calculated voltage under rated load is 481.1 V.

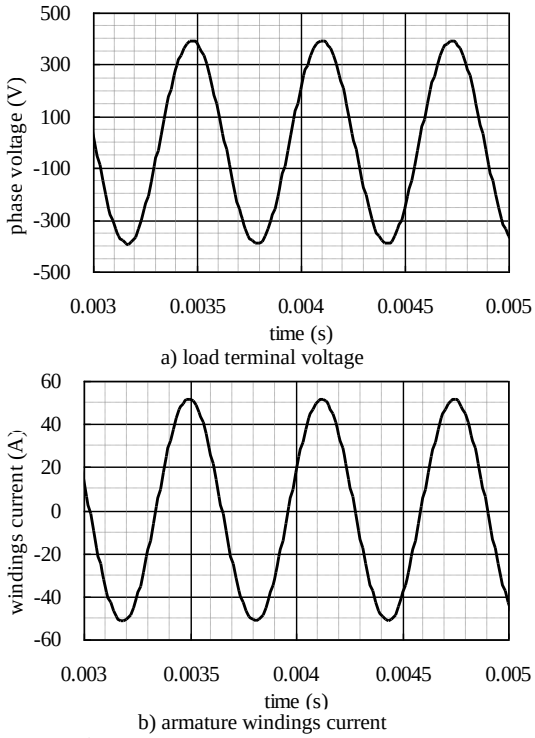

Fig. 2 Variation of machine terminal voltage and armature current with time.

When HSPMG is operating under no-load condition, the air-gap flux density distributes approximately as a flat top wave, which is mainly affected by stator tooth harmonics. Whereas during the rated load operating, the armature reaction magnetic field increases air-gap flux density harmonic components, which also causes eddy loss in rotor sleeve. Meanwhile, the composed main magnetic flux is reduced, as well as the flux density in stator teeth and yoke. Affected by the stator armature field, the composed magnetic pole in teeth is moved compared with that of the no-load situation, and flux density becomes lower and distributes more asymmetrically. Whereas for the flux distribution in yoke, there is nearly no changes, and only the amplitude reduces slightly compare to no-load operation. As shown in Fig.3, the no-load and load flux density distributions in stator core.

To verify the calculation, a HSPMG prototype with similar structure is experimental studied, and the calculated electromagnetic properties under different operating conditions are compared with the measured values, as shown in Table. I. The calculated results show good agreements with the experimental data. In Table I, the errors of voltage and current are smaller than 5%, thus, the accreditation can be inferred.

According to the Law of Electromagnetic Induction, when the closed conductor is relatively moving with a magnetic

filed in perpendicular direction, an electromotive force and current would be induced in the closed conductor. In addition, the caused electrical loss could be calculated as

$$P = I^2R = J^2S_r^2R, \quad (2)$$

where, P is loss (in W), I is the induce current in conductor (in A), J eddy current density (in A/m^2), S_r is conductor area (in m^2), R is resistance (in Ω).

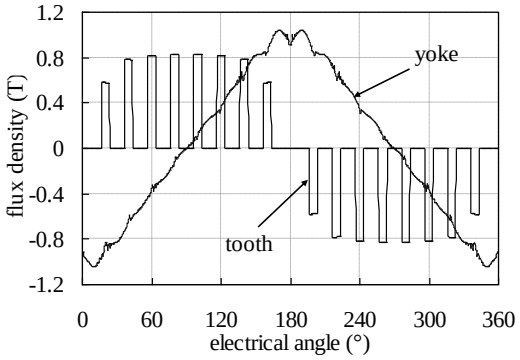

a) no-load flux density wave

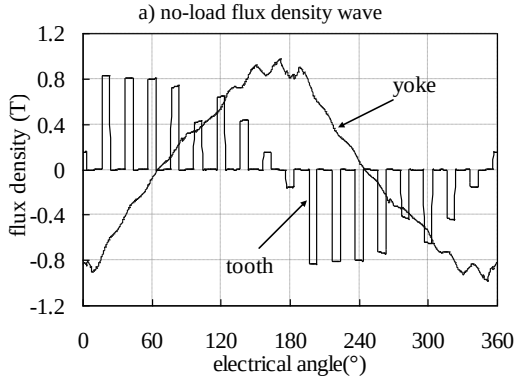

b) load flux density wave

Fig. 3 Comparison of load and no-load flux distributions in HSPMG stator

TABLE I
COMPARISONS OF CALCULATED RESULTS WITH THE EXPERIMENTAL DATA

speed (rpm)	load (Ω)	Test data		Calculated results			
		Phase voltage (V)	Phase current (A)	Phase voltage (V)	error (%)	Phase current (A)	error (%)
10000	2.94	65.1	22.1	66.80	1.1	22.50	1.8
3000	4.96	19.0	4.4	19.90	4.7	4.38	-0.5
3000	1.25	18.5	14.7	18.70	1.1	14.80	0.7
2400	4.96	15.6	3.1	15.21	-2.5	3.02	-2.6
2400	1.87	15.3	8.3	15.16	-0.9	8.23	-0.8
1500	4.96	9.8	1.9	9.55	-2.6	1.93	1.6
1500	1.87	9.6	5.2	9.46	-1.5	5.06	-2.7

Based on the above analyses, the time-varying cycle Te of eddy current density in each element is obtained. If k steps are calculated in a time cycle Te, the eddy loss P_{eddy} in sleeve caused by the stator windings armature magneto-motive force (MMF) and tooth harmonic MMF can be determined as

$$P_{eddy} = \frac{1}{\mathrm{Te}}\int_{\mathrm{Te}} P\mathrm{d}t = \frac{1}{\mathrm{k}}\sum_{i=1}^{\mathrm{k}}\sum_{e=1}^{\mathrm{m}} J_{ie}^2\Delta_e\sigma_r^{-1}l_t, \quad (3)$$

where, J_{ie} is element eddy current density in element e at step i (in A/m^2), Δ_e is element area (in m^2), l_t is sleeve length (in m), σ_r is rotor sleeve conductivity (in S/m), and m is the element amount in sleeve region.

According to [22], the total friction losses on the rotor outer surface and shaft outer surface is determined as 43.8 W. The friction loss in the oil lubricated Ceramic Ball Bearing is 60.1W, but the bearings have a small own self water-cooling system. Thus, in the machine thermal analysis, its thermal effects are ignored.

Add to the electromagnetic losses (the eddy loss and the iron loss) obtained from above analyses, the loss distribution in HSPMG under rated operating is determined, as shown in Table. II, which are taken as the distributed heat generation sources in the fluid-thermal coupling analysis. In the table, the eddy loss in rotor sleeve is determined as 69.7 W from numerical method, which could not be accuracy calculated by the analytical method.

TABLE II
COMPARISON OF RESULTS FROM NUMERICAL CALCULATION AND ANALYTICAL METHOD

	Analytical method	Numerical method	error
Armature current (in A)	36.1	36.3	0.5%
Terminal Voltage (line in V)	480	479.5	-0.1%
Output power (in kVA)	30	30.1	0.3%
Total iron loss (in W)	453.36	442.75	-3%
Copper loss (in W)	250.2	253	1.1%
Rotor eddy loss (in W)	------	69.7	-------

III. TEMPERATURE DISTRIBUTION IN AIR COOLED HSPMG

A. Modeling for thermal-fluid analysis

The HSPMG operates in the inlet channel of a MGTPS. It has an air-cooling ventilation network, in which two air flowing paths parallel distributed. The outer air flowing paths are composed of the grooves formed by the shell outer surfaces and the supporting ribs, whereas the inner paths are mainly of the machine air-gap. Thus, the inlet air of the turbine could cool machine stator core, rotor, and end windings directly. Fig. 4 shows the detail fluid network in the HSPMG. In order to investigate the fluid flowing status and the heat transmission ability of the air-cooling ventilation system, the HSPMG is fluid-thermal coupled analyzed in this section, and the associated factors that affect temperature distribution within the machine are investigated.

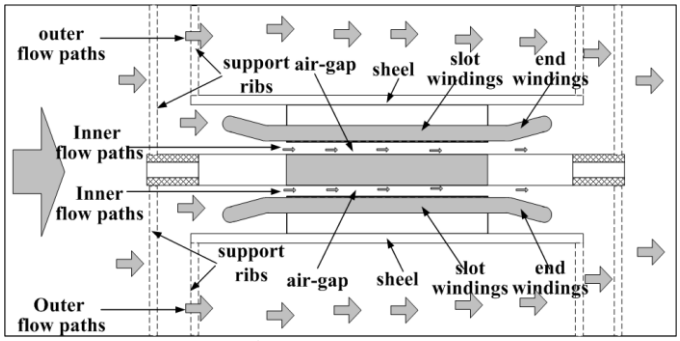

Fig. 4 Ventilation network of air cooling HSPMG.

Considering the air-cooling network structure, based on the fluid dynamic and heat transfer theories, following assumptions are proposed [19].

a) The effects of aerostatics buoyancy and gravity on fluid flowing are ignored.

b) For the moving speed of cooling air is much less the sound velocity, the fluid is considered uncompressible in this analysis.

Thus, the mathematical model for whole region HSPMG fluid-thermal coupling analysis could be determined as

$$\begin{cases} \nabla\cdot(\rho\mathbf{u})=0 \\ \rho\mathbf{F}+\nabla\mathbf{p}+\dfrac{\mu}{3}\nabla(\nabla\cdot\mathbf{u})+\mu\nabla^2\mathbf{u}=0 \\ \nabla\cdot(\rho\mathbf{u}T)=\nabla\cdot(\dfrac{\lambda}{c}\nabla T)+S_T \end{cases}, \tag{4}$$

where, ρ is the fluid density (in kg/m^3); $\mathbf{u}$ is the velocity vector (in m/s); $\mathbf{p}$ is the fluid pressure; μ is the kinematic viscosity (in kg/m·s); T is temperature (in ℃); λ is thermal conductivity [in W/(m·℃)]; c is mass heat capacity [in J/(kg·℃)]; S_T is the heat source density in fluid (in W/m^3).

Because the fluid is following in turbulent states, the standard k–ε model is adopted to calculate the turbulent flow. In the subsequent turbulent flow model, the following Boltzmann equations of kinetic energy of turbulent flow k and diffusion factor ε are used [15]

$$\begin{cases} \dfrac{\partial}{\partial t}(\rho k)+\nabla\cdot(\rho k\mathbf{u})=\nabla\cdot[(\mu+\dfrac{\mu_t}{\sigma_k})\nabla k]+G_k-\rho\varepsilon \\ \dfrac{\partial}{\partial t}(\rho\varepsilon)+\nabla\cdot(\rho\varepsilon\mathbf{u})=\nabla\cdot[(\mu+\dfrac{\mu_t}{\sigma_\varepsilon})\nabla\varepsilon]+C_{1\varepsilon}G_k\dfrac{\varepsilon}{k}-C_{2\varepsilon}\rho\dfrac{\varepsilon^2}{k} \end{cases}, \tag{5}$$

where, G_k is the generation rate of the turbulent flow, μ_t is the turbulent viscosity coefficient, $C_{1\varepsilon}$ and $C_{2\varepsilon}$ are constants, and σ_k and σ_ε are Planck constants of turbulent flow, t is the time.

Fig.5 shows the calculation model for fluid-thermal coupling analysis on HSPMG. In this model the fluid velocity and temperature, determined by the inlet airflow of micro-turbine, are applied as the inlet boundary conditions. For the outlet condition, the natural out flow is adopted. Whereas on the outer surfaces of channel, the natural heat convection condition is applied.

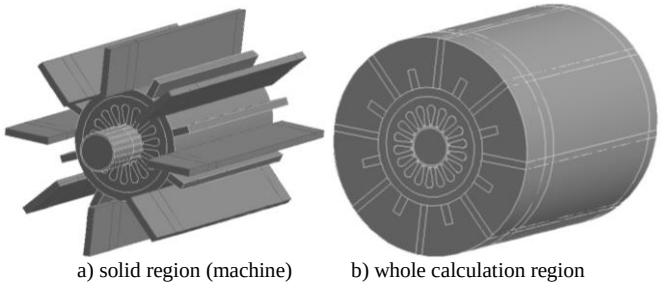

a) solid region (machine) b) whole calculation region

Fig. 5 Analysis model and its elements for HSPMG fluid-thermal coupling study.

In this study, the hexahedron is chosen as the element shape, and 122069 nodes and 110418 elements are meshed in the fluid and solid region grid. The centerline along the shaft is the symmetric axis and the rotating center. Rotor and shaft are with rotating elements (rotor elements in Fig.6), which are rotating in an angular velocity of 10053.1 rad/s, whereas the air-gap is with stationary elements.

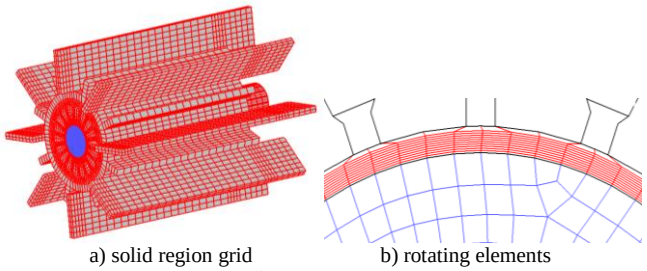

a) solid region grid b) rotating elements

Fig. 6 Elements distribution in fluid-thermal coupling analysis model.

B. Electro-thermal-fluid coupled calculation

The material electrical conductivity, permeability, particularly the permanent magnets working performance varies with temperatures, which affect machine operating performance and temperature distribution. During the coupling calculation, the influences of working temperature on the electromagnetic and the thermal properties of materials in HSPMG are considered via a temperature iteration process.

At the beginning of the iteration, the initial ambient temperature (T_{is} =25℃) is assumed as the working temperature, and the electromagnetic and the thermal characteristics of various materials (including the magnets) are considered to be the ones at such temperature. Through the electromagnetic field calculation, the losses distributions are obtained, which are transferred to the fluid-thermal coupled analyses. A new temperature distribution is determined, and the working temperatures of materials in different machine components are also obtained. Then, replace the initial assumed temperatures (T_{is}) of machine different components by the calculated ones (T'_{is}), and all the electromagnetic-fluid-thermal calculation will be done iteratively, until the maximum relative temperature difference (ΔT) between T_{is} and T'_{is} is less than the requirements (0.5%). The temperature iteration calculation flow is shown as Fig.7.

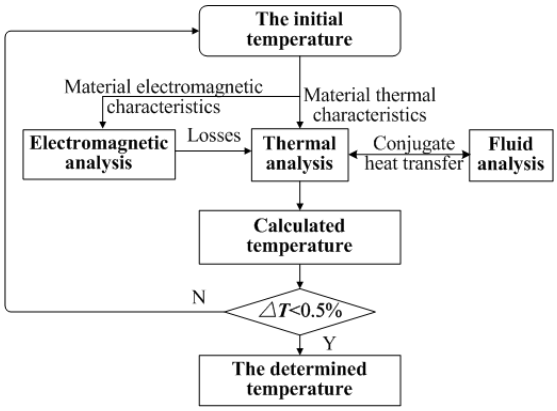

Fig. 7. Electro-thermal-fluid coupling iteration flowchart.

C. Temperature distribution in HSPMG

During the rated operating, the rotational speed of rotor is 96000 rpm, and the rotor peripheral speeds reaches up to 160 m/s. The moving velocity distributions of air in the inner flow paths are showing in Fig. 8. Fig.8 a) shows the tangential velocity of moving air along the radial direction from rotor outer surface to stator inner surface. From the variation curve, it can be seen that the tangential velocity reduces to 60 m/s rapidly within the region of 0.1 mm from rotor outer surface, and then reduces slowly until to 0 m/s at stator inner surface.

When the inlet fluid speed is 20 m/s, the calculated axial speed of cooling air in air-gap is shown in Fig.8 b). Because of the larger wind drag, most of the cooling air through the outer flow paths, and the velocity and the quantity of fluid in the inner flow paths are relatively low. In the figure, the average velocity of air-gap fluid is only 11.7 m/s.

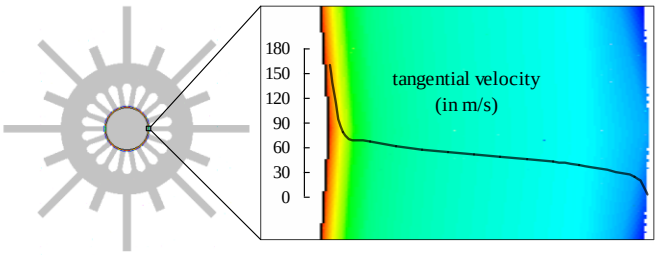

a) tangential velocity

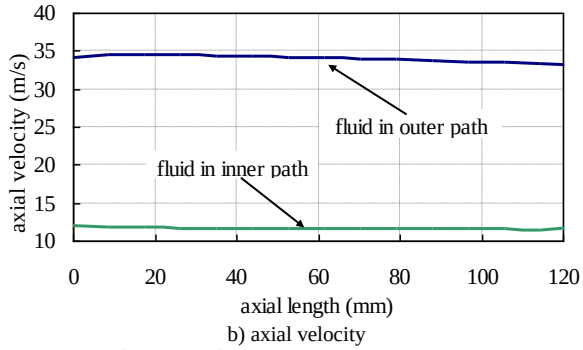

b) axial velocity

Fig. 8 Variation of velocity of cooling air in air-gap.

Fig.9 shows the distribution of heat transfer coefficient on the contact surfaces between the solid region and the fluid region. The heat transfer coefficient streamline distributed on the support ribs surfaces along the axial direction and it changes according to the fluid flowing state. When the inlet velocity of fluid is 20 m/s, the maximum heat coefficients reaches 106 [W/(m^2℃)]. The heat transfer coefficients on the ribs surfaces that corresponding to core region are larger than that of other locations. The average heat transfer coefficient on machine shell outer surface is higher than that of rib surfaces.

From the coupling analyses, the temperature distributions in HSPMG are also obtained, which are shown in Fig.10. At different axial positions, the temperature distributes symmetrically. The highest temperature locates at rotor, and it reaches up to 158.85 ℃. The lowest temperature appears on the cooling air at the entrance of the inlet channel.

Along the axial direction, the temperature of cooling air increases from ventilation system inlet to its outlet, and the heat transfer ability of the cooling air reduces gradually. Thus, the temperature increases obviously along the axial direction and the axial highest temperature appears at rotor body near the cooling outlet. On the supporting ribs, the highest temperature locates at the position connect to shell, which reduces gradually along the radial direction, and some clear temperature belts are formed.

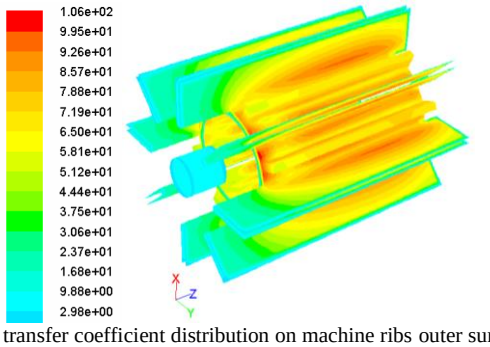

Fig. 9 Heat transfer coefficient distribution on machine ribs outer surfaces [in W/(m^2·℃)].

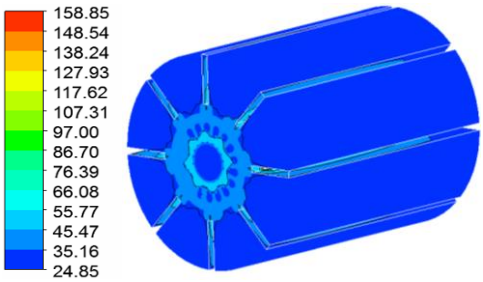

a) temperature distribution in fluid region

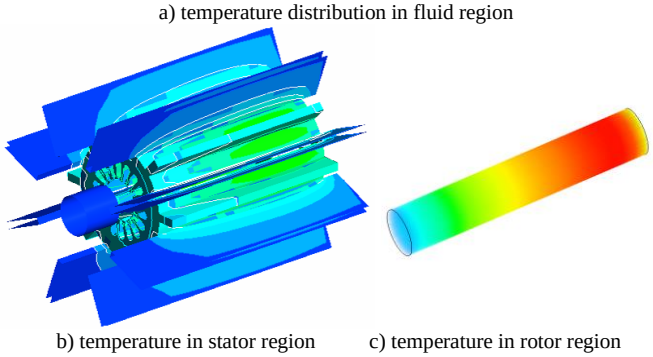

b) temperature in stator region c) temperature in rotor region

Fig. 10 Temperature distribution in HSPMG with air cooling system (in ℃).

IV. ELECTRO-THERMAL COUPLING OPTIMAL DESIGN OF SLOT NOTCH HEIGHT

For the air-cooling HSPMG, the change of slot notch would

affect machine electromagnetic performance and loss distributions, because of the change of main magnetic circuit. On the other hand, the inner flow paths would also change as slot notch, which influence the cooling network and working temperature distribution inside HSPMG. Thus, in this paper, the stator notch is optimized considering the electromagnetic and thermal performance comprehensively.

A. Variations of HSPMG electromagnetic performance with slot notch height

The air-gap flux density harmonics in HSPMG with different notch height (H_k) are shown in Fig.11, from which it can be seen that the variations of different order flux density harmonic are slightly as the notch height increasing. In the partial enlarge figure, the first and the second slot harmonics (the 17th, the 19th, the 35th, and the 37th harmonics of air-gap flux) are obvious larger than the nearby order harmonics, which would cause more eddy loss in rotor sleeve. As H_k increasing the first order slot harmonic reduces slightly.

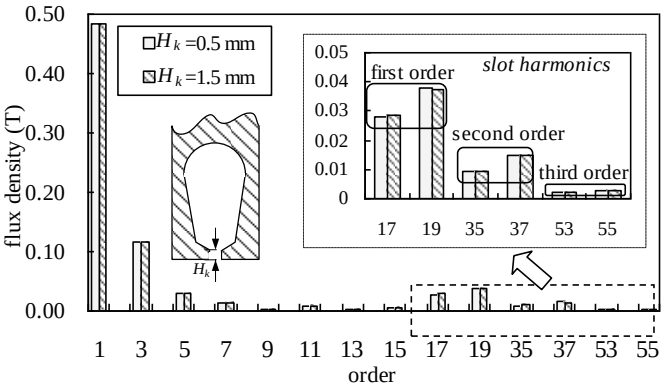

Fig. 11 Flux density harmonics in air-gap of HSPMG with different H_k.

With a fixed stator outer diameter, the width of machine yoke is decreasing as H_k increasing, which may make the flux density in yoke higher and cause a larger core loss. The variation of stator core loss is shown in Fig.12. A higher notch height promotes the reduction of eddy loss in rotor sleeve caused by armature reaction magnetic field. On the other hand, the decrease of stator armature current also makes the armature reaction magnetic flux reduced. Thus, the reduction of eddy losses in rotor is influenced by above two reasons. In Fig.13, the rotor eddy loss reduces about 3.9% when H_k rise from 0.5mm to 1.5mm.

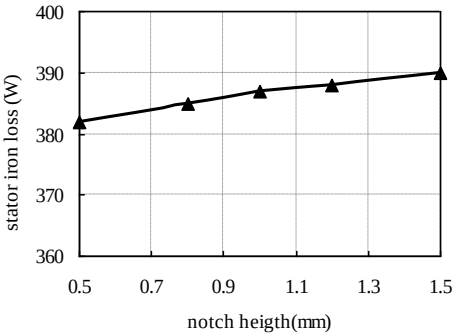

Fig. 12 Variation of stator core loss with H_k

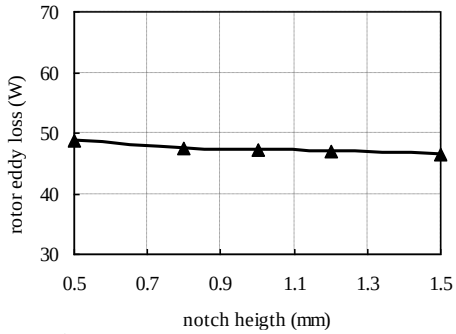

Fig. 13 Variation of rotor eddy loss with H_k.

The increment of slot notch height would make teeth wider if rests of the dimensions of HSPMG are kept the same. The flux density in stator teeth decrease slightly may lower the machine back EMF and the terminal voltage. Meanwhile, the high flux density region at tooth top becomes larger, and it promotes the total iron loss in stator core. Consequently, the efficiency of HSPMG reduces 0.09%, when slot notch rise from 0.5 mm to 1.5 mm. The detail performance parameters of machine with different slot notch heights are list in Table III.

TABLE III
COMPARISONS OF ELECTROMAGNETIC PARAMETERS OF HSPMG WITH DIFFERENT NOTCH HEIGHT

Notch height (mm)	0.5	0.8	1.0	1.2	1.5
Armature current (A)	35.92	35.71	35.50	35.36	35.21
Line voltage (V)	473.96	470.29	469.07	467.84	464.17
Output power (kVA)	29.48	29.09	28.84	28.65	28.31
Copper loss(W)	244.74	244.83	241.93	240.0	238.09
Stator iron loss(W)	382	385	387	388	390
Rotor eddy loss(W)	69.7	68.5	68.4	67.5	67.0
efficiency（%）	97.61	97.58	97.56	97.55	97.52

Based on the HSPMG electromagnetic performance data that change as slot notch height list in Table III, by using high order polynomial analytic function fitting, a series analytical equations to describe performance parameters variations are obtained, in which the slot notch H_k is taking as the variables. During the data proceeding, the ratio between SSE (the sum of squares due to errors between the fitting data and the original data) and SST (the total sum of squares between the original data and its mean value) is less than 0.0008, thus, the coefficients of determination about this curve fitting is greater than 0.9992. The obtained equations are shown as

$$\begin{cases} f_u(H_k) = 481.6 - 20.08 * H_k + 10.82 * H_k^2 - 3.34 * H_k^3 \\ f_i(H_k) = 37.01 - 3.181 * H_k + 2.48 * H_k^2 - 0.7832 * H_k^3 \\ f_p(H_k) = 30840 - 3808 * H_k + 2652 * H_k^2 - 827.9 * H_k^3 \\ f_{pi}(H_k) = 372.4 + 25.94 * H_k - 15.9 * H_k^2 + 4.285 * H_k^3 \\ f_{pe}(H_k) = 71.48 - 4.084 * H_k + 0.9325 * H_k^2 \\ f_{eff}(H_k) = 97.63 - 0.03615 * H_k - 0.02522 * H_k^2 \end{cases} \quad (6)$$

where, $f_u(H_k)$ is the function of stator terminal voltage(in V), $f_i(H_k)$ is the function of armature current (in A), $f_p(H_k)$ is the function of out put power (in VA), $f_{pi}(H_k)$ is the function of stator iron loss (in W), $f_{pe}(H_k)$ is the function of

rotor eddy loss (in W), $f_{eff}(H_k)$ is the function of HSPMG efficiency (in percentage), H_k is slot notch height (in mm), $0< H_k <2$。

B. Temperature in HSPMG with different slot notches

In this paper, the variations of both the cooling fluid heat transmission state and the temperature distributions caused by the stator slot notch height change are investigated. Fig.14 shows the distributions of air-gap cooling air axial velocity. Along with the increasing of stator slot notch height, the effective flowing space for cooling air in air-gap is becoming larger which enhance the cooling air mass flow in inner flow paths. Thus, the axial moving velocity and heat transfer ability of cooling medium are increased. In the same cooling air inlet case, the partial back flow increases when cooling air enter air-gap over the bearing.

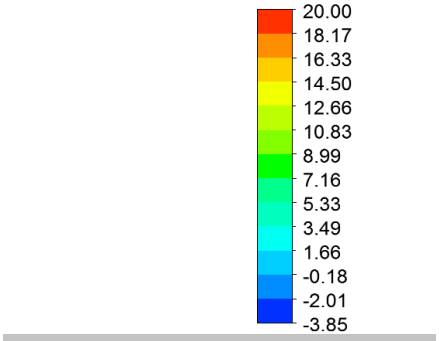

a) H_k = 0.5mm

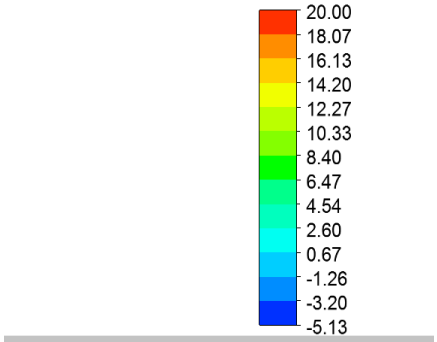

b) H_k = 1.0mm

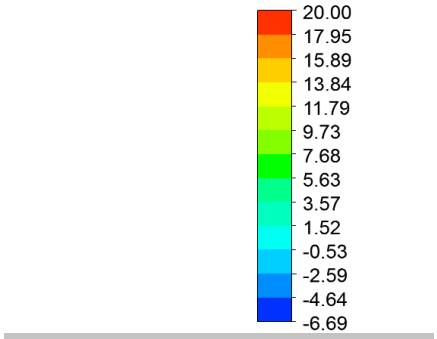

c) H_k = 1.5mm

Fig. 14 Axial speed of air in air-gap of HSPMG with H_k (in m/s).

Fig.15 shows the axial velocity of the flowing air between support ribs. In the entrance region, the velocity changes obvious and several velocity gradient belts appear clearly in the figure. Whereas in the region corresponding to machine

core, the velocity differences of cooling air are very small, although the value is comparatively higher. Comparing the velocity distributions, the influences on cooling air between ribs caused by slot notch height changing are very small, and the variations of velocity are smaller than 0.5 m/s.

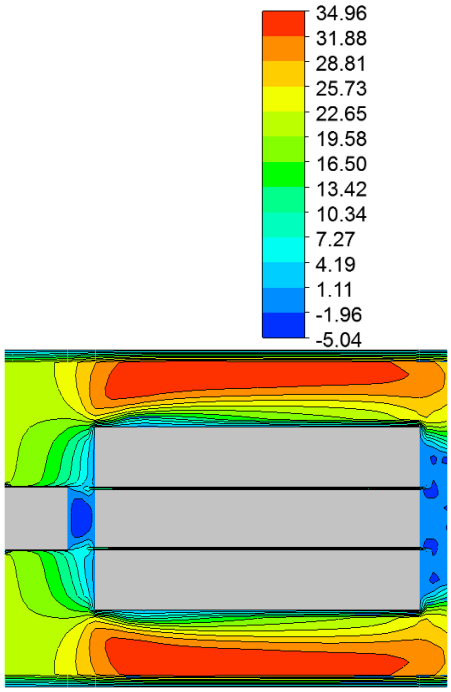

a) H_k = 0.5mm

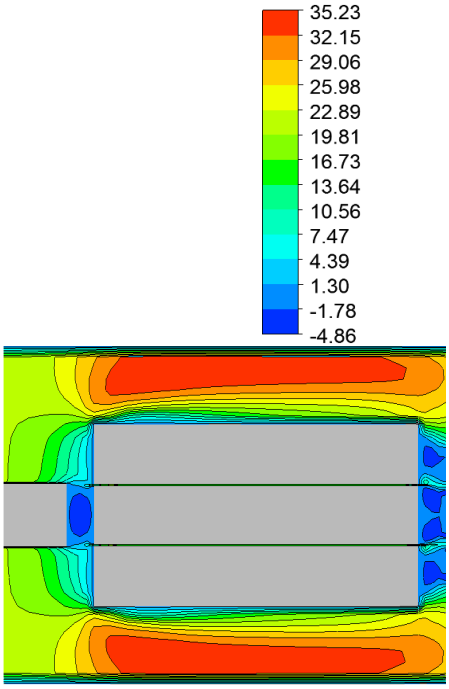

b) H_k = 1.0mm

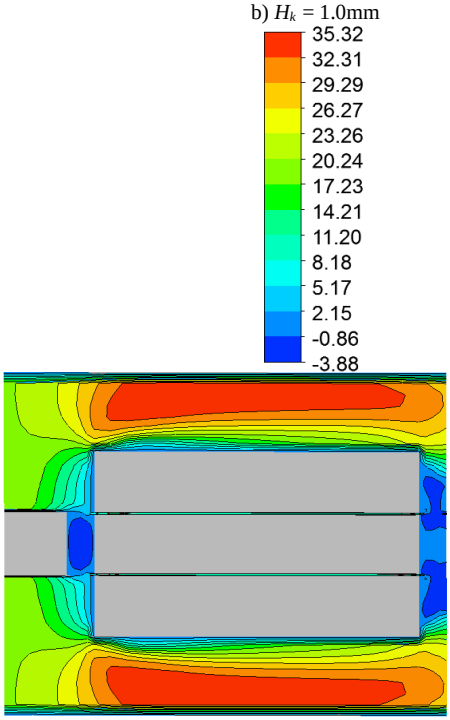

c) H_k = 1.5mm

Fig. 15 Axial velocity of air between fins of HSPMG with H_k (in m/s).

Considering the variations of loss distribution and heat transmission conditions comprehensively, the temperature

distributions in HSPMG with different slot notch height are studied, as shown in Fig.16. The figures describe the temperature gradient distributions in the axial longitudinal section. In the figures, the temperatures inside HSPMG are increasing along the axial direction from cooling air inlet to its outlet, and it decreases obviously within the outlet end region affected by the outlet end cooling air. Thus, the highest temperature appears at rotor with a distance of 20 mm from the outlet end. Because of the large thermal resistance of air-gap, at the same axial position, the rotor temperature is always higher than that in stator, and the axial temperature gradient in rotor is obvious larger. In different slot notch height cases, the temperature distributes circumferential symmetrically at the axial cross section where the highest temperature located. In the whole HSPMG region the highest temperature locates at rotor, and the temperature of the equivalent windings is comparatively higher in stator region.

The effects of slot notch height on the highest temperature of rotor could be obtained from previous equations (6). When the notch height H_k increases from 0.5 mm to 1.5 mm, the highest rotor temperature decreases from 159℃ to 134℃. From former analyses, it can be known that the terminal voltage and efficiency are reduced as slot notch height increase, although it could promotes the reduction of rotor temperature dramatically. Therefore, when HSPMG is kept a constant output power, such effects would weaken.

$$T_r(H_k) = 161 + 3H_k - 14H_k^2 \quad (7)$$

where, T_r is the function of rotor highest temperature (in ℃).

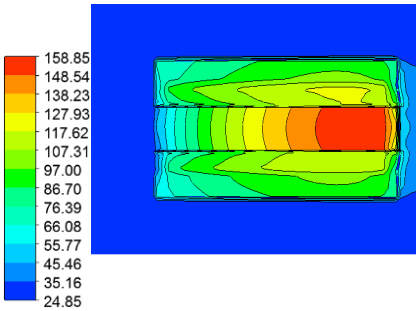

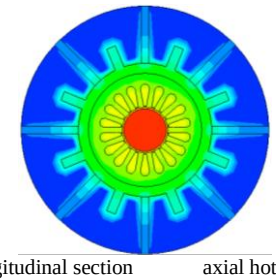

axial longitudinal section axial hottest section

a) H_k = 0.5mm

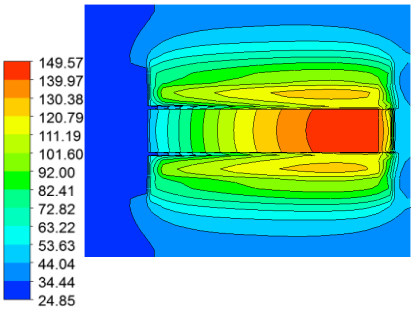

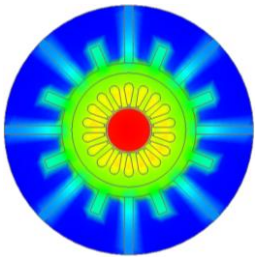

axial longitudinal section axial hottest section

b) H_k = 1.0mm

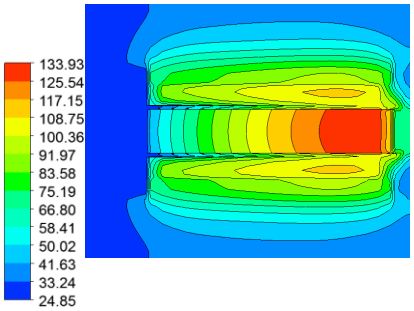

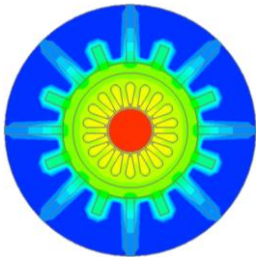

axial longitudinal section axial hottest section

c) H_k = 1.5mm

Fig. 16 Temperature distribution of HSPMG with different H_k (in ℃).

C. Electro-thermal combined optimization on slot notch

In the optimization, the first requirement should be the satisfaction of the terminal voltage and the output power, and other performance should also be considered accordingly. So in the objective function establishment, the unequal weighting coefficients ω are adopted.

Considering the independence of performance parameters in the established functions above, the functions of the stator terminal voltage, the output power, the stator iron loss, the rotor eddy loss, and rotor working temperature are taken as the objective functions. Meanwhile, to avoid the influences of the numerical size differences among machine different performance physical parameters, a relative parameter optimization method is introduced, in which the performance

values of HSPMG under rated operating are taken as the basic standard ones to modify the weighting coefficients. By using such non-equilibrium relative weighting coefficients, the solution of each sub-objective function becomes a dimensionless value.

Integrating the thermal performance objective and the electromagnetic performance objective, a combined optimization model on slot notch aim at electromagnetic and thermal performance is proposed, which could be written as

$$\max F'(H_k) = \omega \cdot Bs_N{}^T \cdot F(H_k)^T, \quad (8)$$

where, $\omega = [\omega_1, \omega_2, \omega_3, \omega_4, \omega_5]$,

$$Bs_N = [\frac{1}{U_N}, \frac{1}{P_N}, \frac{1}{P_{rotor}}, \frac{1}{P_{score}}, \frac{1}{T_r}],$$

$$F(H_k) = [f_u(H_k), f_p(H_k), f_{pe}(H_k), f_{pi}(H_k), T_r(H_k)] \cdot$$

U_N is the rated voltage, P_N is the rated output power, P_{rotor} and P_{score} are the rotor eddy loss and the stator core loss of HSPMG under rated operating, respectively.

Constraint condition are $F(H_k) > 0$, and $0 < H_k < 2$.

By using the Genetic Algorithm (GA)[17], the objective function is processed solved. A fitness function (9) is established according to the GA and objective function.

$$\mathrm{Fit}(H_k) = -\max F'(H_k) \quad (9)$$

where, $0 < H_k \leq 2$。

In the optimizing process, defines the initial population m=30, and the evolution generation is 30. The scattered disorder data cross method (probability=0.65), the Gaussian mutation strategy (probability=0.05), and the former direction migration patterns are adopted. After several iterative calculations, the minimum value of the fitness function could be obtained, which is also the desired maximum value of objective function within the constrain region. When the weighting coefficient ω is [0.8, 0.8, -0.1, -0.25, -0.25], the variation curves of both the optimal fitness value and the average fitness value are shown in Fig.17. At the tenth iteration such two fitness values are -0.9710 and -0.97101, respectively. Thus the optimal value of objective function could be considered as 0.9710, and the corresponding variable H_k is 1.6959.

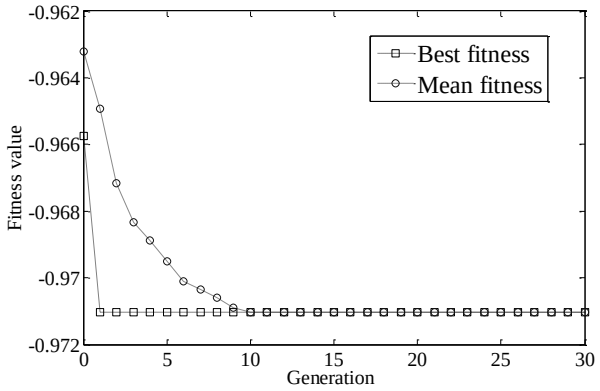

Fig. 17 Curves of fitness in GA iteration process.

To verify the obtained results, the HSPMG with the optimized slot notch height is analyzed via the proposed electromagnetic-fluid-thermal coupling method. The obtained performance parameters from two methods are list in Table IV, in which the objective parameters determined by GA are close to those obtained from numerical analyses. The maximum difference between the two groups is rotor temperature, which is only 0.84 ℃.

The HSPMG studied in this manuscript is with a power level of 30 kVA, and its allowed operating region is within 8%, and the allowed machine line voltage change is within 5%. By using the optimized stator notch height 1.6959 mm, as shown in Table IV, the terminal voltage is 462.37 V, and the output power is 28.21 kVA/27.97 kW, which still satisfy the requirements. The efficiency of machine reduces from 97.62% to 97.51%, and it is larger than the request 97.5%. On the other hand, the highest temperature of rotor reduced about 20.6%, which would enhance the thermal stability of machine significantly. Therefore, considering the both electromagnetic and thermal cases, the optimal slot notch height could promote a better performance of HSPMG.

TABLE IV
COMPARISONS OF THE OPTIMIZED AND THE NUMERICAL CALCULATED PARAMETERS

	Numerical Calculated	GA Optimized	Error
Armature current (A)	35.13	35.23	0.28%
Machine line voltage (V)	461.77	462.37	0.13%
Output power (kVA)	28097	28213	0.41%
Copper loss(W)	391.96	391.56	-0.10%
Iron loss(W)	236.97	238.30	0.56%
Rotor eddy loss(W)	66.8	67.0	0.30%
Efficiency (%)	97.505	97.521	0.02%
Rotor temperature(℃)	124.99	125.83	0.67%

V. CONCLUSION

In this paper, the slot notch of an air cooled HSPMG is optimized aim to enhance both the electromagnetic and the thermal performance, based on the electromagnetic-fluid-thermal coupling analyses. In the process, the effects of slot notch height on magnetic circuit and ventilation path are studied comprehensively, and a non-equilibrium relative weighting method is proposed to modify the optimization function. Thus, an optimal slot notch height of 1.7 mm is determined.

ACKNOWLEDGMENT

This work is supported by the Fundamental Research Funds for the Central Universities of China under Grant 2014JBM115.

REFERENCES

[1] J. B. Ahn, Y. H. Jeong, D. H. Kang, and J. H. Park, "Development of high speed PMSM for distributed generation using microturbine", *In Proc .IEEE Annual Conference of Industrial Electronics Society*, Busan, South Korea, 2-6 Nov, 2004, vol. 3, pp. 2879-2882.

[2] P. Chudi, "Development of a small gas turbine driven high-speed permanent generator", Ph.D. Dissertation. Stockholm, The Royal Institute of Technology, 1989, pp. 25-37.

[3] M. A. Rahman, A. Chiba, T. Fukao. "Super high speed electrical machines-summary". *Power Engineering Society General Meeting*, June 6-10, 2004, Colorado USA, vol.2, pp.1272-1275.

[4] James Borg Bartolo, He Zhang, David Gerada, Liliana De Lillo and Chris Gerada. "High speed electrical generators, application, materials and design", *IEEE Workshop on Electrical Machines Design Control and Diagnosis (WEMDCD)*, 2013, pp. 47-59.

[5] S. Niu, S. L. Ho, W. N. Fu, Z. Jian Guo. "Eddy Current Reduction in High-Speed Machines and Eddy Current Loss Analysis with Multi slice Time-Stepping Finite-Element Method". *IEEE Trans. on Magn.*, 2012, Vol. 48, No. 2, pp. 1007-1010.

[6] D. A. G. Vieira, A. C. Lisboa, R. R. Saldanha. "An Enhanced Ellipsoid Method for Electromagnetic Devices Optimization and Design". *IEEE Transactions on Magn.*, 2010, Vol. 46, No. 8, pp. 2843-2851.

[7] C. Bianchini, F. Immovilli, E. Lorenzani, A. Bellini, M. Davoli. "Review of Design Solutions for Internal Permanent-Magnet Machines Cogging Torque Reduction". *IEEE Trans. on Magn.*, 2012, 46(10): 2685-2693.

[8] H. Do-Kwan, W. Byung-Chul, L. Ji-Young, K. Dae-Hyun. "Ultra High Speed Motor Supported by Air Foil Bearings for Air Blower Cooling Fuel Cells". *IEEE Trans. on Magn.*, 2012, Vol. 48, No. 2, pp. 871-874.

[9] M. Mirzaei, A. Binder, B. Funieru, M. Susic. "Analytical Calculations of Induced Eddy Currents Losses in the Magnets of Surface Mounted PM Machines with Consideration of Circumferential and Axial Segmentation Effects". *IEEE Trans. on Magn.*, 2012, Vol. 48, No. 12, pp. 4831-4841.

[10] David Gerada, Abdeslam Mebarki, Neil L. Brown, Keith J. Bradley, and Chris Gerada. "Design Aspects of High-Speed High-Power-Density Laminated-Rotor Induction Machines", *IEEE Trans. Ind. Electron.*, vol. 58, no. 9, pp. 4039-4047, Sep. 2011.

[11] A. Boglietti, R. I. Bojoi, A. Cavagnino, P. Guglielmi, A. Miotto. "Analysis and Modeling of Rotor Slot Enclosure Effects in High Speed Induction Motors", *IEEE Trans. Ind. Appl.*, vol. 48, no. 4, pp. 1279-1287, Sep. 2012.

[12] F. Marignetti, V. Delli Colli, Y. Coia. "Design of axial flux PM synchronous machines through 3-D coupled electromagnetic thermal and fluid-dynamical finite-element analysis". *IEEE Trans. Ind. Electron.*, vol. 55, no. 10, pp.3591-3601, Oct. 2008.

[13] L. Weili, Z. Xiaochen, C. Shukang, C. Junci, and Z. Yihuang. "Thermal analysis of high speed PM generator", *Science China Technological Science*, vol. 55, no. 5, pp.1419-1426, May. 2012.

[14] Xie Ying. Performance evaluation and thermal fields analysis of induction motor with broken rotor bars located at different relative positions. *IEEE Trans. on Magn.*, 2010, Vol. 46, No. 5, pp. 1243-1250.

[15] G. Traxler-Samek, R. Zickermann, and A. Schwery. "Cooling airflow, losses, and temperatures in large air-cooled synchronous machines". *IEEE Trans. Ind. Electron.*, vol. 57, no. 1, pp. 172-180, Journey, 2010.

[16] L. Weili, C. Junci, and Z. Xiaochen. "Electro-thermal analysis of induction motor with compound cage rotor used for PHEV", *IEEE Trans. Ind. Electron.*, vol. 57, no. 2, pp. 660-668, Feb. 2010.

[17] H. Mirahki, M. Moallem, S. Rahimi. "Design Optimization of IPMSM for 42V Integrated Starter-Alternator using Lumped Parameter Model and Genetic Algorithms". *IEEE Trans. on Magn.*, to be published.

[18] L. Weili, Z. Xiaochen, C. Shukang, and C. Junci. "Thermal Optimization for a HSPMG Used for Distributed Generation Systems", *IEEE Trans. Ind. Electron.*, vol. 60, no. 2, 2013.

[19] C. C. Hwang, S. S. Hung, C. T. Liu, S. P. Cheng. "Optimal Design of a High Speed SPM Motor for Machine Tool Applications". *IEEE Trans. on Magn.*, to be published.

[20] LongHai Special Steel- 50Mn18Cr5 [Online]. Available: http://www.17-4ph.cn/50Mn18Cr5.html.

[21] Professional Material- SmCo magnet [Online]. Available: http://www.profma.com/smco1.htm.

[22] C. Huynh, Z. Liping, D. Acharya, "Losses in high speed permanent magnet machines used in microturbine applications". *Journal of Engineering for Gas Turbines and Power*, vol. 131 /022301-1-6, Mar. 2009.

Zhang. Xiaochen (S'09-M'12) graduated from Harbin University of Science and Technology and received Master's Degree in 2006. He graduated from Harbin Institute of Electrical Technology and received Doctor's Degree in 2012.

He is with the college of Electrical Engineering, Beijing Jiaotong University, Beijing, China. His research interests include research on electromagnetic and thermal analysis on electrical machine, especially in permanent magnetic machines.

Li. Weili (ICS Number) graduated from Harbin Institute of Electrical Technology and received Master's Degree in 1993. He graduated from Russia Electric Power Research Institute and received Doctor's Degree in 1997.

He is currently a professor in the college of Electrical Engineering, Beijing Jiaotong University, Beijing, China. He is the author or coauthor of more than 200 published refereed technical papers and he also holds 22 patents. His research interests include synthesis physical field analyses on large electrical machines, renewable energy systems, and special electrical machine and associate control.